A Hard-Constraint Time-Stepping Approach for Rigid Multibody Dynamics with Joints, Contact, and Friction

Gary D. Hart*
Department of Mathematics
University of Pittsburgh
Thackeray 301
Pittsburgh, PA 15260
gdhart@pitt.edu

Mihai Anitescu
Mathematics and Computer Science Division
Building 221, Argonne National Laboratory
9700 South Cass Avenue
Argonne, IL 60439
anitescu@mcs.anl.gov

ABSTRACT

We present a method for simulating rigid multibody dynamics with joints, contact, and friction. In this work, the nonsmooth contact and frictional constraints are represented by hard constraints. The method requires the solution of only one linear complementarity problem per step and can progress at much larger time steps than explicit penalty methods, which are currently the method of choice for most of these simulations.

Categories & Subject Descriptors: G.1.7 [Ordinary Differential Equations]: Differentiall-algbraic equations; J.2 [Physical Sciences and Engineering]: Mathematics and Statistics, Physics, Engineering; I.6.3 [Applications]

General Terms: Performance, Experimentation,Theory.

Keywords: Numerical Analysis, Complementarity Problems, Rigid Body Dynamics, Friction, Contact Problems.

Subject Index 65L80, 90C33, 70E55, 74M10, 74M15

1. INTRODUCTION

Simulating the dynamics of a system with several rigid bodies and with joint, contact (noninterpenetration), and friction constraints is an important part of virtual reality and robotics simulations.

If the simulation has only joint constraints, then the problem is a differential algebraic equation (DAE) [19, 10]. However, the nonsmooth nature of the noninterpenetration and friction constraints requires the use of specialized techniques. Approaches used in the past for simulating rigid multibody dynamics with contact and friction include piecewise DAE approaches [19], acceleration-force linear complementarity problem (LCP) approaches [17, 11, 28], penalty (or regularization) approaches [15, 25], and velocity-impulse LCP-based time-stepping methods [27, 26, 5, 7]. When the value of the time step is set to 0, the LCP of the velocity-impulse approach is the same as the one used in the compression phase of multiple collision resolution [18].

Of all these approaches the penalty approach is probably the most frequently encountered in the mechanical engineering literature. It accommodates the nonsmooth nature of contact and friction by smoothing their mathematical descriptions. The advantage of this approach is that it is easy to set up and results in a DAE, for which both analytical and software tools are in a fairly mature state of development. The disadvantages are that finding *a priori* appropriate values for the smoothing parameters is difficult and that it results a very stiff problem even for moderate time steps.

The LCP method represents both contact and friction as inequality constraints that are computationally treated as hard constraints. The advantage of this method is that there are no extra parameters to tune and no artificial stiffness. It may therefore be expected to work better with less user input. On the other hand, the subproblems are now constrained by inequalities, and separate analysis and software tools need to be developed to make the approach successful.

In this work we use the velocity-impulse LCP-based approach, which has the advantage that it does not suffer from the lack of a solution that can appear the piecewise DAE and acceleration-force LCP approach [11, 26]. It also does not suffer from the artificial stiffness that is introduced by the penalty approach. In previous work, we have shown how to approach stiffness [6].

In previous work we have shown that the method [2] achieves geometrical (noninterpenetration and joint) constraint stabilization for complementarity-based time-stepping methods for rigid multibody dynamics with contact, joints, and friction. A variant of the scheme presented here is currently used for the dynamical simulation of dynamical robotic grasps [21, 4]. This scheme needs no computational effort other than that for solving the basic LCP subproblem, though the free term of the LCP is modified compared with other time-stepping LCP approaches [6, 5, 27].

The constraint stabilization issue in a complementarity setting has been tackled by using nonlinear complementarity problems [27], an LCP followed by a nonlinear projection approach that includes nonlinear inequality constraints [6], and a postprocessing method [12] that uses one potentially nonconvex LCP based on the stiff method developed

*Address all correspondence to this author

TAPIA'03, October 15–18, 2003, Atlanta, Georgia, USA.

in [6] followed by one convex LCP for constraint stabilization. When applied to joint-only systems, the method from [12] belongs to the set of postprocessing methods defined in [9, 8]. In order to achieve constraint stabilization, however, all of these methods need additional computation after the basic LCP subproblem has been solved. This stands in contrast with our approach, which needs no additional computational effort to achieve constraint stabilization.

2. THE LINEAR COMPLEMENTARITY SUBPROBLEM OF THE TIME-STEPPING SCHEME

In this section, we review a velocity-impulse LCP-based time-stepping scheme that uses an Euler discretization [5, 27]. In the following, q and v constitute, respectively, the generalized position and generalized velocity vector of a system of several bodies [19].

2.1 Model Constraints

Throughout this subsection we use **complementarity notation**. If $a, b \in I\!R$, we say that a is complementary to b, and we denote it by $a \perp b$ or $a \geq 0 \perp b \geq 0$ if $a \geq 0$, $b \geq 0$, and $ab = 0$.

2.1.1 Geometrical Constraints

Joint constraints (2.1) and noninterpenetration constraints (2.3) involve only the position variable and depend on the shape of the bodies and the type of constraints involved. We call them geometrical constraints.

Joint Constraints. Joint constraints are described by the equations

$$\Theta^{(i)}(q) = 0,\ i = 1, 2, \ldots, m\,. \tag{2.1}$$

Here, $\Theta^{(i)}(q)$ are sufficiently smooth functions. We denote by $\nu^{(i)}(q)$ the gradient of the corresponding function, or

$$\nu^{(i)}(q) = \nabla_q \Theta^{(i)}(q), \quad i = 1, 2, \ldots, m. \tag{2.2}$$

The impulse exerted by a joint on the system is $c_\nu^{(i)} \nu^{(i)}(q)$, where $c_\nu^{(i)}$ is a scalar related to the Lagrange multiplier of classical constrained dynamics [19].

Noninterpenetration Constraints. Noninterpenetration constraints are defined in terms of a continuous signed distance function between the two bodies $\Phi^{(j)}(q)$ [1]. The noninterpenetration constraints become

$$\Phi^{(j)}(q) \geq 0, \quad j = 1, 2, \ldots, p. \tag{2.3}$$

The function $\Phi^{(j)}(q)$ is generally not differentiable everywhere. We discuss sufficient conditions for local differentiability of $\Phi^{(j)}(q)$ in [2]. In the following, we refer to j as the *contact* j, although the contact is truly active only when $\Phi^{(j)}(q) = 0$. We denote the normal at contact (j) by

$$n^{(j)}(q) = \nabla_q \Phi^{(j)}(q), \quad j = 1, 2, \ldots, p. \tag{2.4}$$

When the contact is active, it can exert a compressive normal impulse, $c_n^{(j)} n^{(j)}(q)$, on the system, which is quantified by requiring $c_n^{(j)} \geq 0$. The fact that the contact must be active before a nonzero compression impulse can act is expressed by the complementarity constraint

$$\Phi^{(j)}(q) \geq 0 \perp c_n^{(j)} \geq 0, \quad j = 1, 2, \ldots, p. \tag{2.5}$$

Differentiability properties. The mappings $\Theta^{(i)}(q)$ that define the joint constraints are differentiable [19]. The situation, is different, however, for the mapping defining the noninterpenetration constraints. The mappings $\Phi^{(j)}(q)$ cannot be differentiable everywhere, in general, no matter how simple or regular the shape of the bodies [2]. If the bodies are smooth and relatively strictly convex, then the mapping $\Phi^{(j)}(q)$ is differentiable as long as the interpenetration value is not large [1]. The mappings $\Phi^{(j)}(q)$ are obviously not differentiable for bodies with nonsmooth shapes.

To simplify our analysis, we assume that the mappings that define the joint and noninterpenetration constraints are differentiable. If the shapes are such that the mappings $\Phi^{(j)}(q)$ are differentiable only for small values of the interpenetration, then the analysis of this work can be extended, in a straightforward though laborious manner, as in [2] to demonstrate the constraint stabilization effect.

Since any body can be approximated by a finite union of convex, smooth-shaped bodies, we could extend, in principle, the analysis in this work for approximation of any configuration. Probably, however, it is computationally more efficient to accommodate nonsmooth or nonconvex shapes directly, by working with a piecewise smooth mapping $\Phi^{(j)}$. We defer the analysis of this situation to future research.

2.1.2 Frictional Constraints

Frictional constraints are expressed by means of a discretization of the Coulomb friction cone [6, 5, 27]. For a contact $j \in \{1, 2, \ldots, p\}$, we take a collection of coplanar vectors $d_i^{(j)}(q)$, $i = 1, 2, \ldots, m_C^{(j)}$, which span the plane tangent at the contact (though the plane may cease to be tangent to the contact normal when mapped in generalized coordinates [1]). The convex cover of the vectors $d_i^{(j)}(q)$ should approximate the transversal shape of the friction cone. In two-dimensional mechanics, the tangent plane is one dimensional, its transversal shape is a segment, and only two such vectors $d_1^{(j)}(q)$ and $d_2^{(j)}(q)$ are needed in this formulation. We denote by $D^{(j)}(q)$ a matrix whose columns are $d_i^{(j)}(q) \neq 0$, $i = 1, 2, \ldots, m_C^{(j)}$, that is, $D^{(j)}(q) = \left[d_1^{(j)}(q), d_2^{(j)}(q), \ldots, d_{m_C^{(j)}}^{(j)}(q) \right]$. A tangential impulse is $\sum_{i=1}^{m_C^{(j)}} \beta_i^{(j)} d_i^{(j)}(q)$, where $\beta_i^{(j)} \geq 0$, $i = 1, 2, \ldots, m_C^{(j)}$. We assume that the tangential contact description is balanced, that is,

$$\forall 1 \leq i \leq m_C^{(j)},\ \exists k,\ 1 \leq k \leq m_C^{(j)} \text{ such that } d_i^{(j)}(q) = -d_k^{(j)}(q). \tag{2.6}$$

The friction model ensures maximum dissipation for given normal impulse $c_n^{(j)}$ and velocity v and guarantees that the total contact force is inside the discretized cone. We express this model as

$$\begin{array}{rcl} D^{(j)^T}(q) v + \lambda^{(j)} e^{(j)} & \geq 0 \quad \perp \quad \beta^{(j)} \geq 0, \\ \mu c_n^{(j)} - e^{(j)^T} \beta^{(j)} & \geq 0 \quad \perp \quad \lambda^{(j)} \geq 0. \end{array} \tag{2.7}$$

Here $e^{(j)}$ is a vector of ones of dimension $m_C^{(j)}$, $e^{(j)} = (1, 1, \ldots, 1)^T$, $\mu^{(j)} \geq 0$ is the Coulomb friction parameter, and $\beta^{(j)}$ is the vector of tangential impulses $\beta^{(j)} =$

$\left(\beta_1^{(j)}, \beta_2^{(j)}, \ldots, \beta_{m_C^{(j)}}^{(j)}\right)^T$. The additional variable $\lambda^{(j)} \geq 0$ is approximately equal to the norm of the tangential velocity at the contact, if there is relative motion at the contact, or $\left|\left|D(q)^{(j)^T} v\right|\right| \neq 0$ [5, 27].

Notation. We denote by $M(q)$ the symmetric, positive definite mass matrix of the system in the generalized coordinates q and by $k(t, q, v)$ the external force. All quantities described in this section associated with contact j are denoted by the superscript $^{(j)}$. When we use a vector or matrix norm whose index is not specified, it is the 2 norm.

2.2 The Linear Complementarity Problem

Let $h_l > 0$ be the time step at time $t^{(l)}$, when the system is at position $q^{(l)}$ and velocity $v^{(l)}$. We have that $h_l = t^{(l+1)} - t^{(l)}$. We choose the new position to be $q^{(l+1)} = q^{(l)} + h_l v^{(l+1)}$, where $v^{(l+1)}$ is determined by enforcing the simulation constraints.

The geometrical constraints are enforced at the velocity level by linearization of the mappings $\Theta^{(i)}$ and $\Phi^{(j)}$. For joint constraints the linearization leads to

$$\begin{aligned} \Theta^{(i)}(q^{(l)}) + h_l \nabla_q \Theta^{(i)^T}(q^{(l)}) v^{(l+1)} &= \\ \Theta^{(i)}(q^{(l)}) + h_l \nu^{(i)^T}(q^{(l)}) v^{(l+1)} &= 0, \quad i = 1, 2, \ldots, m. \end{aligned} \tag{2.8}$$

For a noninterpenetration constraint of index j, $\Phi^{(j)}(q) \geq 0$, linearization at $q^{(l)}$ for one time step amounts to $\Phi^{(j)}(q^{(l)}) + h_l \nabla_q \Phi^{(j)^T}(q^{(l)}) v^{(l+1)} \geq 0$; that is, after including the complementarity constraints (2.5) and using the definition of $n^{(j)}(q^{(l)})$, we have

$$n^{(j)^T}(q^{(l)}) v^{(l+1)} + \frac{\Phi^{(j)}(q^{(l)})}{h_l} \geq 0 \perp c_n^{(j)} \geq 0. \tag{2.9}$$

For computational efficiency, only the contacts that are imminently active are included in the dynamical resolution and linearized, and their set is denoted by $\mathcal{A}$. One practical way of determining $\mathcal{A}$ is by including all j for which $\Phi^{(j)}(q) \leq \hat{\epsilon}$, where $\hat{\epsilon}$ is a sufficiently small quantity.

When using the relation (2.9) to model contact, we may obtain a nonconvex linear complementarity subproblem which may be difficult to solve [3]. To alleviate this difficulty, one can use an approach that results in a convex linear complementarity problem, that is, in effect, equivalent to a quadratic program [3]. The approach consists in replacing the linearized problem (2.9) by

$$n^{(j)^T}(q^{(l)}) v^{(l+1)} + \frac{\Phi^{(j)}(q^{(l)})}{h_l} - \mu^{(j)} \lambda^{(j)} \geq 0 \perp c_n^{(j)} \geq 0. \tag{2.10}$$

When using (2.10) to model contact, we call the approach *the optimization approach*. Naturally, in using this approach we modify the dynamics. Nevertheless, the distance between the solution of the dynamics of the original approach (2.9) and the relaxed approach (2.10) is bounded above by a constant times the maximum of the quantitites $\mu^{(j)} \lambda^{(j)}$ [3]. Therefore, in the case of low friction or low tangential slip, which often occurs in practice, the error will be small. Moreover, optimization-based relaxations for contact and friction are interesting in themselves and have found applications in graphics [20] and nonsmooth frictional dynamics [23].

If a collision occurs, then a collision resolution, possibly with energy restitution, needs to be applied [18, 5]. In our setup a collision occurs at step l for a contact j if the first inequality in (2.9) is satisfied with equality, and at step $l-1$ it was satisfied as a strict inequality.

In this work we assume that no energy lost during collision is restituted; hence we avoid the need to consider a compression LCP followed by decompression LCP [5]. The relation (2.9) is sufficient to accommodate totally plastic collisions.

To completely define the LCP subproblem, we use an Euler discretization of Newton's law, which results in the following equation:

$$\begin{aligned} M(q^{(l)}) \left(v^{(l+1)} - v^{(l)}\right) &= h_l k\left(t^{(l)}, q^{(l)}, v^{(l)}\right) \\ &+ \textstyle\sum_{i=1}^{m} c_\nu^{(i)} \nu^{(i)}(q^{(l)}) + \\ \textstyle\sum_{j \in \mathcal{A}} \left(c_n^{(j)} n^{(j)}(q^{(l)}) \right. &+ \left. \textstyle\sum_{i=1}^{m_C^{(j)}} \beta_i^{(j)} d_i^{(j)}(q^{(l)})\right). \end{aligned}$$

After collecting all the constraints introduced above, with the geometrical constraints replaced by their linearized versions (2.8) and (2.9), we obtain the following mixed LCP:

$$\begin{bmatrix} M^{(l)} & -\widetilde{\nu} & -\widetilde{n} & -\widetilde{D} & 0 \\ \widetilde{\nu}^T & 0 & 0 & 0 & 0 \\ \widetilde{n}^T & 0 & 0 & 0 & 0 \\ \widetilde{D}^T & 0 & 0 & 0 & \widetilde{E} \\ 0 & 0 & \widetilde{\mu} & -\widetilde{E}^T & 0 \end{bmatrix} \begin{bmatrix} v^{(l+1)} \\ c_\nu \\ c_n \\ \widetilde{\beta} \\ \lambda \end{bmatrix} + \begin{bmatrix} -M v^{(l)} - h_l k^{(l)} \\ \Upsilon \\ \Delta \\ 0 \\ 0 \end{bmatrix} = \begin{bmatrix} 0 \\ 0 \\ \rho \\ \widetilde{\sigma} \\ \zeta \end{bmatrix} \tag{2.11}$$

$$\begin{bmatrix} c_n \\ \widetilde{\beta} \\ \lambda \end{bmatrix}^T \begin{bmatrix} \rho \\ \widetilde{\sigma} \\ \zeta \end{bmatrix} = 0, \qquad \begin{bmatrix} c_n \\ \widetilde{\beta} \\ \lambda \end{bmatrix} \geq 0, \qquad \begin{bmatrix} \rho \\ \widetilde{\sigma} \\ \zeta \end{bmatrix} \geq 0\,. \tag{2.12}$$

Here $\widetilde{\nu} = [\nu^{(1)}, \nu^{(2)}, \ldots, \nu^{(m)}]$, $c_\nu = [c_\nu^{(1)}, c_\nu^{(2)}, \ldots, c_\nu^{(m)}]^T$, $\widetilde{n} = [n^{(j_1)}, n^{(j_1)}, \ldots, n^{(j_s)}]$, $c_n = [c_n^{(j_1)}, c_n^{(j_2)}, \ldots, c_n^{(j_s)}]^T$, $\widetilde{\beta} = [\beta^{(j_1)^T}, \beta^{(j_2)^T}, \ldots, \beta^{(j_s)^T}]^T$, $\widetilde{D} = [D^{(j_1)}, D^{(j_2)}, \ldots, D^{(j_s)}]$, $\lambda = [\lambda^{(j_1)}, \lambda^{(j_2)}, \ldots, \lambda^{(j_s)}]^T$, $\widetilde{\mu} = diag(\mu^{(j_1)}, \mu^{(j_2)}, \ldots, \mu^{(j_s)})^T$, $\Upsilon = \frac{1}{h}\left(\Theta^{(1)}, \Theta^{(2)}, \ldots, \Theta^{(m)}\right)^T$, $\Delta = \frac{1}{h}\left(\Phi^{(j_1)}, \Phi^{(j_2)}, \ldots, \Phi^{(j_s)}\right)^T$ and

$$\widetilde{E} = \begin{bmatrix} e^{(j_1)} & 0 & 0 & \cdots & 0 \\ 0 & e^{(j_2)} & 0 & \cdots & 0 \\ \vdots & \vdots & \vdots & \vdots & \vdots \\ 0 & 0 & 0 & \cdots & e^{(j_s)} \end{bmatrix}$$

are the lumped LCP data, and $\mathcal{A} = \{j_1, j_2, \ldots, j_s\}$ are the active contact constraints. The vector inequalities in (2.12) are to be understood componentwise. We use the $\widetilde{\ }$ notation to indicate that the quantity is obtained by properly adjoining blocks that are relevant to the aggregate joint or contact constraints. The problem is called mixed LCP because it contains both equality and complementarity constraints.

To simplify the presentation, we have not explicitly included the dependence of the parameters in (2.11–2.12) on $q^{(l)}$. Also, $M^{(l)} = M(q^{(l)})$ is the value of the mass matrix at time $t^{(l)}$, and $k^{(l)} = k(t^{(l)}, q^{(l)}, v^{(l)})$ represents the external force at time $t^{(l)}$.

The optimization approach. When (2.10) is used instead of (2.9), the matrix form is the same as (2.11–2.12) except that the block appearing in position (5,3) in (2.11) will be $-\widetilde{\mu}^T$ instead of 0. Insofar as LCP is concerned, the

good properties of the new formulation are evident because the matrix of the LCP is positive semidefinite for this case.

Choice of the active set $\mathcal{A}$ and collision detection. Most previous approaches have a simulate-detect-restart flavor [5, 11, 13, 27]. In these approaches, after the velocity is determined as a solution of the LCP, the simulation does not necessarily progress for the duration of the time step if a collision is encountered. The simulation is stopped at the collision, the collision is resolved by using LCP techniques [18, 5], and the simulation is restarted. For such approaches, the active set is updated as a result of collision detection. If many collisions occur per unit of simulation, then there will be many costly updates that will interfere with the performance of the solver.

In the approach presented here, the active set is defined, with $\hat{\epsilon}$ an appropriately chosen quantity, as

$$\mathcal{A}(q) = \left\{ j | \Phi^{(j)}(q) \leq \hat{\epsilon},\ 1 \leq j \leq p \right\}. \qquad (2.13)$$

In this case there is no need to stop the simulation if $\hat{\epsilon}$ is appropriately chosen. A good guideline for this choice is $\hat{\epsilon} = v_{\max} h$, where h is of the order of the expected size of the time step and v_{max} is the expected range of the velocity. Since the definitions of the active sets are different, the results of computing with our definition of the active set and the simulate-detect-restart strategy [11, 5, 27] will be different.

In [2] we have shown that this scheme achieves constraint stabilization and that infeasibility at step l is upper bounded by $O(||h_{l-1}||^2 \left|\left|v^{(l)}\right|\right|^2)$.

3. NUMERICAL RESULTS FOR CONTACT CONSTRAINTS

To compute our results, we have use the PATH solver [16, 14]. The path solver solves the general linear complementarity problem and, since it implements some version of Lemke's algorithm, it is guaranteed to find a solution for either the LCP formulation or the optimization formulation. In a preceding paper, we have called the optimization formulation LCP3 [3]. We are currently investigating using convex quadratic program solvers instead of PATH for the optimization formulation. Since PATH solves the general linear complementarity problem; it does not exploit symmetry and uses only LU factorization for linear algebra. A QP solver would be able to solve symmetric subproblems, so we expect computational savings even from the linear algebra.

To validate the concepts introduced in the preceding sections, we applied our method where $v^{(l+1)}$ is computed by (2.11–2.12) to two two-dimensional examples, and we compared it with the unstabilized version (which corresponds to the choice $\Delta = 0$, and $\Upsilon = 0$ in (2.11–2.12). We ran both examples for 20 seconds with a time step of 0.05. The mass data corresponds to a density of 10kg/m^2. All computations were done by solving one linear complementarity problem per step, using PATH [14].

We choose $\widehat{\epsilon}$, the parameter that governs the choice of the active set (2.13), to be equal to 0.3. In the limit of $h_l \to 0$, the value of the active set parameter $\hat{\epsilon}$ is not an issue, as proved in [2]. This parameter does influence the efficiency of the algorithm, however, since a larger $\hat{\epsilon}$ means that the size of the LCP (2.11–2.12) will increase. On the other hand, a smaller $\hat{\epsilon}$ means that certain collisions may be missed and could result in a large increase of the infeasibility.

In the first example, we simulate with the LCP method an elliptic body above and on a tabletop. The length of its axes are 8 and 4. The body is dropped from a height of 8 with respect to its center of mass and with an angular velocity of 3. The friction coefficient is 0.3. In Figure 1 we present ten frames of the simulation. In Figure 2 we present a comparison of the constraint infeasibility between the unstabilized and stabilized version of our algorithm. The benefit of the stabilization is evident in the figure where the infeasibility is more than 100 times smaller toward the end of the simulation in the stabilized case compared with the unstabilized case. We also see that in the stabilized case the infeasibility oscillates in a narrow range without exhibiting a substantial increase.

In the second example, we simulate with the LCP method the behavior of 21 identical disks of radius 3 on a horizontal tabletop bounded by two slanted walls, starting from the cannonball arrangement at 0 velocity (with 6 disks at the bottom). The friction coefficient is 0.2. Four frames of the simulation are presented in Figures (3)–(6).

In Figure 8 we compare the constraint infeasibility between the unstabilized and the stabilized method. We see that the stabilized method has smaller constraint infeasibility and consistently corrects incidental large infeasibility. At the end of the simulation, all disks are separated, and they are all in contact with the tabletop. The disk on tabletop constraint is satisfied exactly because it is linear in the region of differentiability, which explains the essentially zero infeasibility in both methods toward the end of the simulation time interval.

In both examples we see that constraint stabilization is achieved by our method, whereas the unstabilized method exhibits a continuous drift in the first example and a larger and more persistent infeasibility in the second example. We also note that in both examples we were able to achieve constraint stabilization by solving only one LCP per step with a constant time step.

In the example of the Brazil nut effect [24], we have smaller particles shaken together with a large particle that, after a while, emerges on top. This is a behavior that is characteristic of granular matter. This effect is seen in four frames of the simulation in Figure 9. That example contains 201 bodies and is simulated with the optimization method for 75 seconds with time step of 0.1s and friction coefficient of 0.5 at all interactions. Our time step compares very favorably with the traditional molecular dynamics approaches that uses a penalty method and that needs time steps on the order of microseconds. The computing time spent using this method and the number of contacts are presented in Figure 7. We do not have currently any molecular dynamics result to compare with, mostly since molecular dynamics simulations use periodic boundary conditions, whereas we use hard walls. In any event, the number of shakes needed to get the larger body emerge to the top is comparable to the number of shakes needed by a molecular dynamics simulation that uses periodic boundary conditions and temperature to model the dynamics of the bodies [24].

Acknowledgments

We thank Michael Ferris and Todd Munson for providing and maintaining PATH [22, 14], a package for solving general linear complementarity problems. This work was performed under the NSF awards DMS-9305760, DMS-0112239, and

Contract No. W-31-109-ENG-38 with the U.S. Department of Energy (Mihai Anitescu) and under a CRDF award from the University of Pittsburgh (Mihai Anitescu and Gary D. Hart).

4. REFERENCES

[1] M. Anitescu, J. F. Cremer, and F. A. Potra. Formulating 3d contact dynamics problems. *Mechanics of Structures and Machines*, 24(4):405–437, 1996.

[2] M. Anitescu and G. D. Hart. A constraint-stabilized time-stepping scheme for multi-body dynamics with contact and friction'. Preprint ANL/MCS-P1002-1002, Argonne National Laboratory, Argonne, Illinois, 2002.

[3] M. Anitescu and G. D. Hart. A fixed-point iteration approach for multibody dynamics with contact and friction. Preprint ANL/MCS-P985-0802, Argonne National Laboratory, Argonne, Illinois, 2002.

[4] M. Anitescu, A. Miller, and G. D. Hart. Constraint stabilization for time-stepping approaches for rigid multibody dynamics with joints, contact and friction. In *Proceedings of the ASME International Design Engineering Technical Conferences*, page to appear. ASME, 2003.

[5] M. Anitescu and F. A. Potra. Formulating dynamic multi-rigid-body contact problems with friction as solvable linear complementarity problems. *Nonlinear Dynamics*, 14:231–247, 1997.

[6] M. Anitescu and F. A. Potra. Time-stepping schemes for stiff multi-rigid-body dynamics with contact and friction. *International Journal for Numerical Methods in Engineering*, 55(7):753–784, 2002.

[7] M. Anitescu, F. A. Potra, and D. Stewart. Time-stepping for three-dimensional rigid-body dynamics. *Computer Methods in Applied Mechanics and Engineering*, 177:183–197, 1999.

[8] U. Ascher, H. Chin, L. Petzold, and S. Reich. Stabilization of constrained mechanical systems with daes and invariant manifolds. *J. Mech. Struct. Mach*, 23:135–158, 1995.

[9] U. Ascher, H. Chin, and S.Reich. Stabilization of daes and invariant manifolds. *Numerische Mathematik*, 67:131–149, 1994.

[10] U. M. Ascher and L. R. Petzold. *Computer methods for ordinary differential equations and differential-algebraic equations*. Society for Industrial and Applied Mathematics, Philadelphia, PA, 1998.

[11] D. Baraff. Issues in computing contact forces for non-penetrating rigid bodies. *Algorithmica*, 10:292–352, 1993.

[12] M. B. Cline and D. K. Pai. Post-stabilization for rigid body simulation with contact and constraints. In *Proceedings of the IEEE International Conference in Robotics and Automation*. IEEE, 2003.

[13] J. F. Cremer and A. J. Stewart. The architecture of newton, a general purpose dynamics simulator. In *Proceedings of the IEEE International Conference in Robotics and Automation*, pages 1806–1811. IEEE, 1989.

[14] S. Dirkse and M. Ferris. The PATH solver: A non-monotone stabilization scheme for mixed complementarity problems. *Optimization Methods and Software*, 5:123–156, 1995.

[15] B. R. Donald and D. K. Pai. On the motion of compliantly connected rigid bodies in contact: a system for analyzing designs for assembly. In *Proceedings of the Conf. on Robotics and Automation*, pages 1756–1762. IEEE, 1990.

[16] M. Ferris and T. Munson. Interfaces to PATH 3.0: Design, implementation and usage. *Computational Optimization and Applications*, 12:207–227, 1999.

[17] C. Glocker and F. Pfeiffer. An lcp-approach for multibody systems with planar friction. In *Proceedings of the CMIS 92 Contact Mechanics Int. Symposium*, pages 13 – 30, Lausanne, Switzerland, 1992.

[18] C. Glocker and F. Pfeiffer. Multiple impacts with friction in rigid multi-body systems. *Nonlinear Dynamics*, 7:471–497, 1995.

[19] E. J. Haug. *Computer Aided Kinematics and Dynamics of Mechanical Systems*. Allyn and Bacon, Boston, 1989.

[20] Milenkovic and Schmidl. *Optimization-based animation*. SIGGRAPH, 2001.

[21] A. Miller and H. I. Christensen. Implementation of multi-rigid-body dynamics within a robotics grasping simulator'. Preprint, Columbia University, http://www.cs.columbia.edu/~amiller/graspit/index.html, 2002.

[22] T. S. Munson. *Algorithms and Environments for Complementarity*. PhD thesis, Department of Computer Science, University of Wisconsin-Madison, Madison, Wisconsin, 2000.

[23] A. Pandolfi, C. Kane, J. E. Marsden, and M. Ortiz. Time-discretized variational formulations of non-smooth frictional contact. *International Journal for Numerical Methods in Engineering*, 53(8):1801–1829, 2002.

[24] A. Rosato, K. Strandburg, F. Prinz, and R. H. Swendsen. Why the brazil nuts are on top: size segregation of particulate matter by shacking. *Physical Review Letters*, 58(10):1038–1040, 1987.

[25] P. Song, P. Kraus, V. Kumar, and P. Dupont. Analysis of rigid-body dynamic models for simulation of systems with frictional contacts. *Journal of Applied Mechanics*, 68(1):118–128, 2001.

[26] D. E. Stewart. Rigid-body dynamics with friction and impact. *SIAM Review*, 42(1):3–39, 2000.

[27] D. E. Stewart and J. C. Trinkle. An implicit time-stepping scheme for rigid-body dynamics with inelastic collisions and coulomb friction. *International Journal for Numerical Methods in Engineering*, 39:2673–2691, 1996.

[28] J. Trinkle, J.-S. Pang, S. Sudarsky, and G. Lo. On dynamic multi-rigid-body contact problems with coulomb friction. *Zeithschrift fur Angewandte Mathematik und Mechanik*, 77:267–279, 1997.

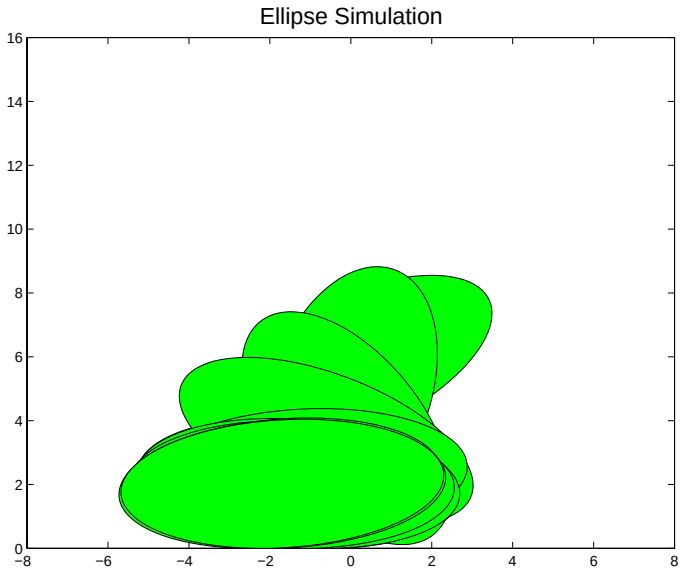

Figure 1: Ten frames of an ellipse on a tabletop simulation.

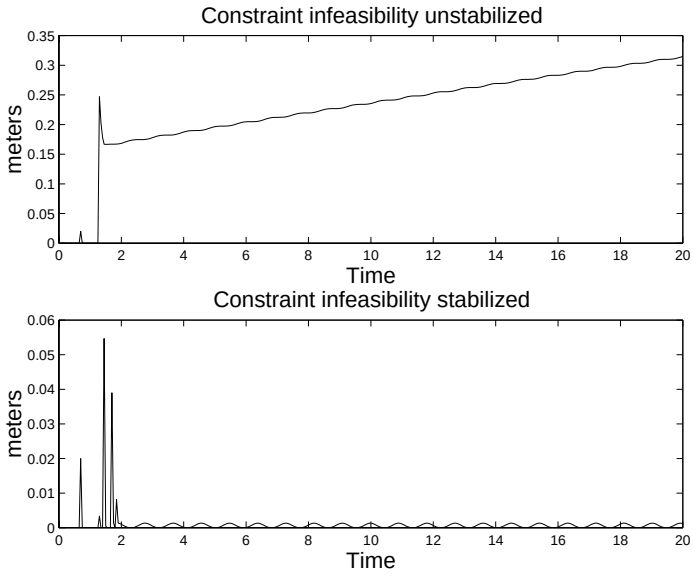

Figure 2: Ellipse simulation: Comparison of the constraint infeasibility between the unstabilized method and the stabilized method.

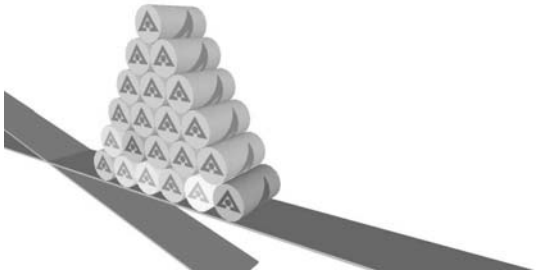

Figure 3: Frame 1 of the simulation.

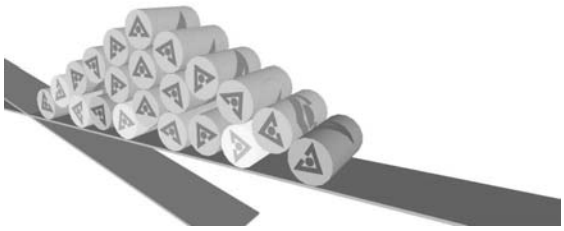

Figure 4: Frame 2 of the simulation.

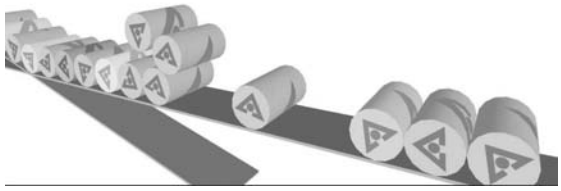

Figure 5: Frame 3 of the simulation.

Figure 6: Frame 4 of the simulation.

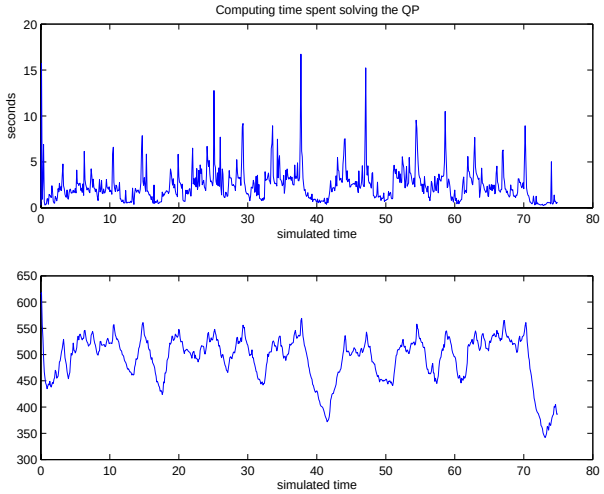

Figure 7: Performance statistics and number of contacts for the Brazil nut simulation

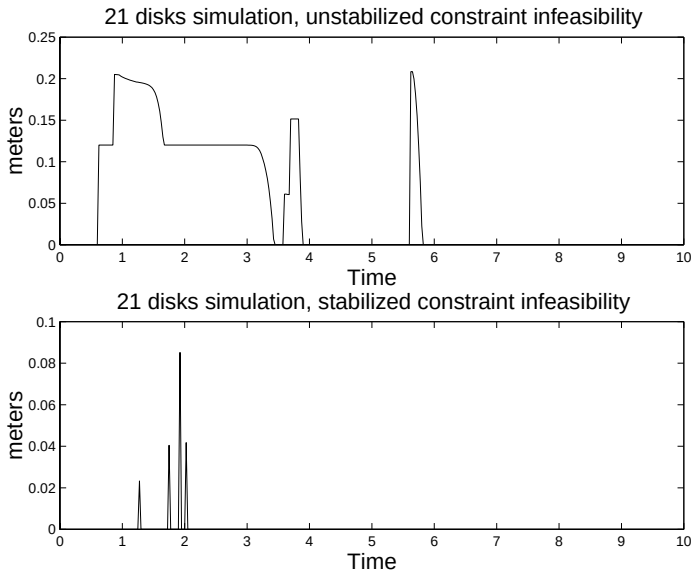

Figure 8: Disks simulation: Comparison of the constraint infeasibility between the unstabilized method and the stabilized method.

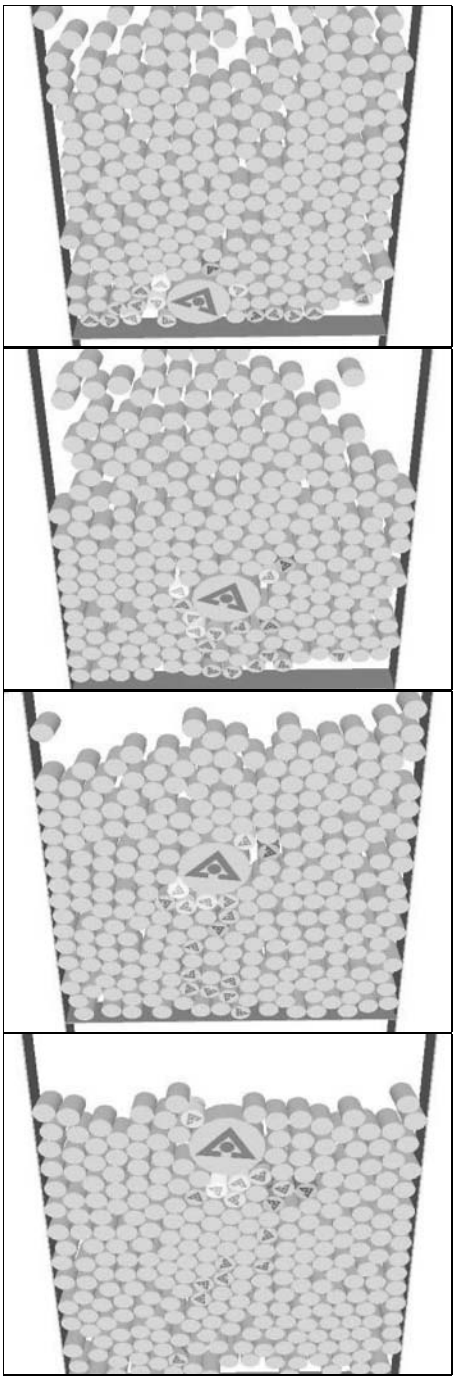

Figure 9: Four frames of a Brazil nut simulation with inelastic collisions